

Investigation of Immobilization Effects on Ni(P₂N₂)₂ Electrocatalysts

Felix M. Brunner, Michael L. Neville, and Clifford P. Kubiak*

Cite This: *Inorg. Chem.* 2020, 59, 16872–16881

Read Online

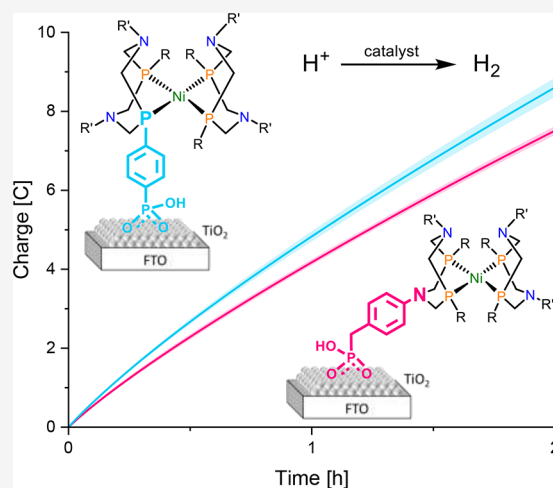
ACCESS |

Metrics & More

Article Recommendations

Supporting Information

ABSTRACT: A new synthetic route to complexes of the type Ni(P₂N₂)₂²⁺ with highly functionalized phosphine substituents and the investigation of immobilization effects on these catalysts is reported. Ni(P₂N₂)₂²⁺ complexes have been extensively studied as homogeneous and surface-attached molecular electrocatalysts for the hydrogen evolution reaction (HER). A synthesis based on postsynthetic modification of P^{ArBr}₂N^{Ph}₂ was developed and is described here. Phosphonate-modified ligands and their corresponding nickel complexes were isolated and characterized. Subsequent deprotection of the phosphonic ester derivatives provided the first Ni(P₂N₂)₂²⁺ catalyst that can be covalently attached via pendent phosphonate groups to an electrode without involvement of the important pendent amine groups. Mesoporous TiO₂ electrodes were surface modified by attachment of the new phosphonate functionalized Ni(P₂N₂)₂²⁺ complexes, and these provided electrocatalytic materials that proved to be competent and stable for sustained HER in aqueous solution at mild pH and low overpotential. We directly compared the new ligand to a previously reported complex that utilized the amine moiety for surface attachment. Using HER as the benchmark reaction, the P-attached catalyst showed a marginally (9–14%) higher turnover number than its N-attached counterpart.



INTRODUCTION

The P₂N₂ (1,5-diaza-3,7-diphosphacyclooctane) class of ligands has been established as a very versatile platform and used with various metals to catalyze a wide variety of different reactions including the oxidations of amines, alcohols, and formate as well as the hydrogen evolution reaction (HER) and the reduction of CO₂.^{1–4} In particular, Ni(P₂N₂)₂ complexes have been widely studied and proven to be exceptional electrocatalysts for HER and H₂ oxidation.⁵ To implement these catalysts in practical electrochemical devices, efficient ways to immobilize them on electrodes while preserving the catalysts' unique properties must be developed. In the past decade, various strategies for the immobilization of Ni(P₂N₂)₂ catalysts onto a variety of support materials ranging from carbon nanotubes to silicon to metal oxide semiconductors were developed.^{6–12} All of the surface-immobilized Ni(P₂N₂)₂ catalysts examined to date have in common the attachment through the amine moieties of the P₂N₂ ligand. This is not optimal in view of mechanistic studies, which have demonstrated the importance of free mobility of the amine groups as “pendent base” proton shuttles in catalysis. Presumably, pinning the pendent base to the surface could adversely affect catalysis.^{13,14} An alternative attachment utilizing the phosphine moiety would be advantageous from this perspective. However, this route was previously not pursued, likely due to synthetic challenges arising from the low

availability and high reactivity of primary phosphines, a key component in the P₂N₂ ligand synthesis. Developing alternative attachment strategies and directly comparing them in a side-by-side study gives clearer insight into how surface attachment affects these catalysts. Herein, we describe the first synthesis of a P₂N₂ complex modified with a surface attachable functional group on the phosphine moiety (**6**; Figure 1). Mesoporous TiO₂ electrodes modified with **6** are functional electrode materials for HER in aqueous solution. Direct comparison of the phosphine anchored catalyst **6** to the previously reported complex **7**¹⁵ anchored through the nitrogen moiety allows us to directly observe the differences caused by changing the surface attachment substituent to the phosphine.

RESULTS AND DISCUSSION

Retrosynthetic Analysis of the Catalyst. Of the many examples of surface-attached P₂N₂ ligands, the most impactful utilize either amide coupling to modified carbon⁶ and gold⁹

Received: June 5, 2020

Published: November 16, 2020



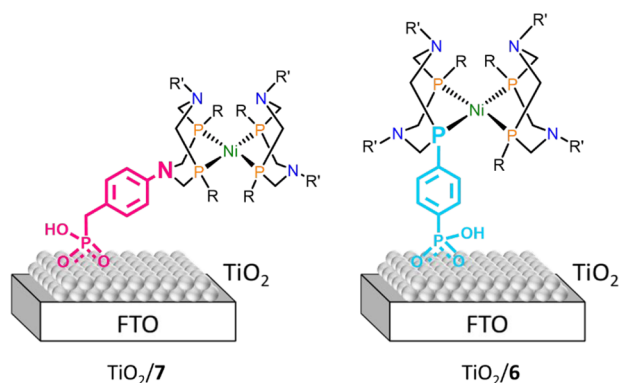


Figure 1. Schematic representation of the two attachment methods of $\text{Ni}(\text{P}_2\text{N}_2)_2$ to a mesoporous TiO_2 electrode. Attachment through a modified amine moiety **7** (left) and through a modified phosphine moiety **6** (right). All R-substituents are benzylphosphonic acid (**7**) or phenylphosphonic acids (**6**) and are omitted for clarity.

electrodes or phosphonate groups for attachment to metal oxide semiconductors.¹⁶ Our method for P-modified P_2N_2 ligands was designed to allow synthetic introduction of both carboxylate and phosphonate substituents for surface attachment. However, due to the harsh conditions necessary to synthesize primary phosphines, it is not possible to directly synthesize primary phosphines with either carboxylic or phosphonic acid substituents. Therefore, an alternative strategy was developed based on postsynthetic modification of the ligands. Since the goal was to introduce substituents in the *para*-position of a phenyl phosphine, we were limited to reactions that can modify aromatics but are compatible with phosphines. This excludes all oxidative reactions or any of those that involve “phosphineophiles”. The most versatile approach to directly modify an aromatic ring is through cross coupling or organolithium reactions, which can be used to introduce a variety of functional groups. A second requirement for the modification is that the precursor group is inert to the harsh reducing conditions necessary to make the primary phosphine while also being unreactive toward that phosphine. Halogens represent a class of functional groups that are commonly used as precursors for further functionalization. Literature precedent suggests that aryl halides are not reactive toward phenyl phosphine.¹⁷ In the presence of LiAlH_4 , both chlorine and fluorine aryl substituents are inert, while phenyl iodide is readily dehalogenated. Aryl bromides were found to react more slowly, and only minor degrees of dehalogenation

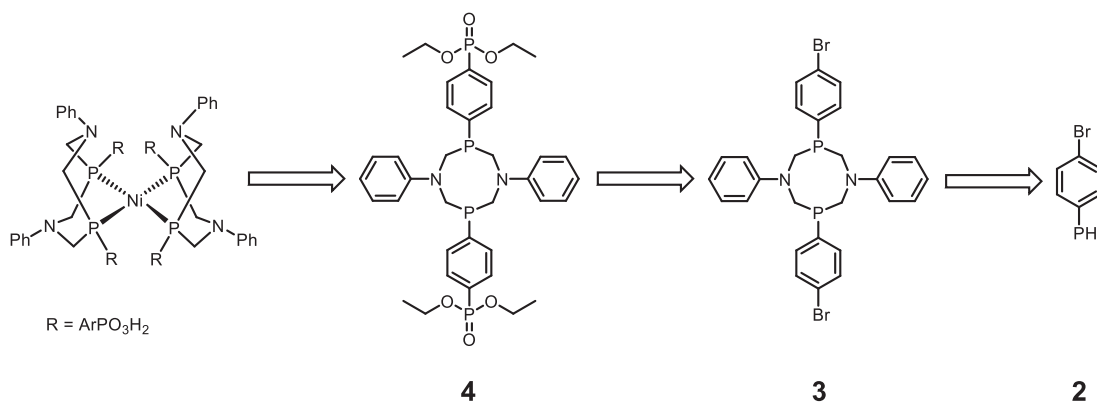
were expected in the reaction to prepare the primary phosphine.¹⁸ The greater versatility of aryl bromides in subsequent modification steps make them the better choice over chlorine. 4-Bromophenylphosphine (**2**) is a stable molecule and can be converted into the corresponding P_2N_2 (**3**; Scheme 1). This makes **3** an ideal intermediate in the synthesis of more functionalized P_2N_2 ligands by postsynthetic functionalization (Scheme 1). This bromine substituted P_2N_2 **3** is converted into the phosphonate ester (**4**; Scheme 1) or other functional groups utilizing lithium chemistry. The functionalized ligand can then be coordinated to the Ni center and deprotected following known procedures.¹⁶

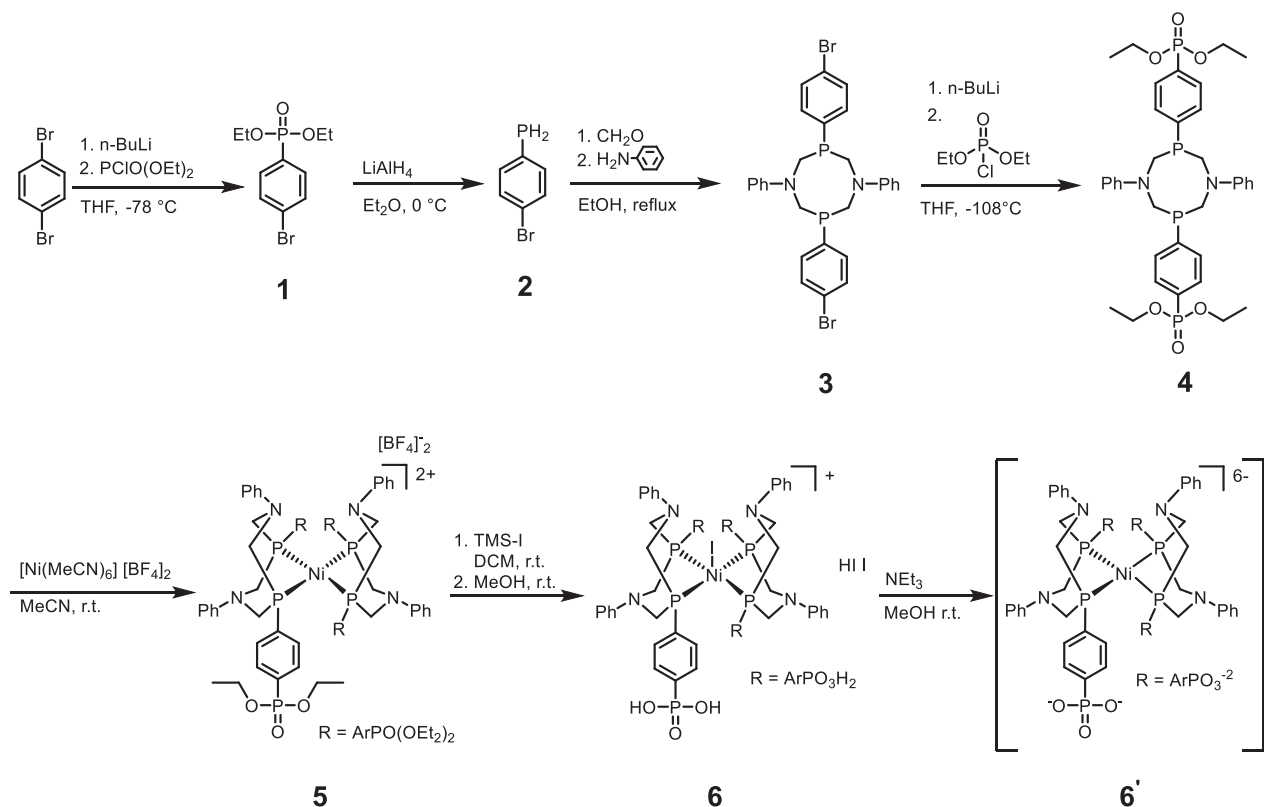
Synthesis and Characterization of $[\text{Ni}(\text{P}^{\text{Ar}}\text{PO}_3\text{H}_2\text{N}^{\text{Ph}})_2][\text{I}] \cdot \text{HI}$. Following the guidance of the retrosynthetic analysis shown in Scheme 1, we developed a synthetic route to the desired complex. Starting from readily available 1,4-dibromobenzene, the primary phosphine 4-bromophenylphosphine (**2**) can be obtained in two steps: introduction of a phosphorus group and subsequent reduction. For the first step, a previous synthesis of diethyl (4-bromophenyl)phosphonate (**1**) was modified to allow for easy scale-up.¹⁹ Selective halogen lithium exchange of one bromine was followed by electrophilic substitution with diethoxychlorophosphonate yielding **1**. The resulting phosphonate ester was then reduced with LiAlH_4 to the corresponding primary phosphine **2**. Following an established procedure²⁰ for P_2N_2 synthesis, **2** was reacted with formaldehyde and aniline to yield the P-bromine substituted ligand $\text{P}^{\text{ArBr}}\text{N}_2^{\text{Ph}}$ (**3**) (Scheme 2).

The bromine functionalized P_2N_2 presents a useful intermediate for further functionalization of the phosphine substituent through postsynthetic modification. Of the possible reactions, lithium chemistry was identified as the cleanest method to exchange the bromine for a phosphonate group (Scheme 2). Attempts to cross couple the bromide derivative in a Suzuki type reaction to further functionalize the ligand were limited by its strong coordination affinity toward transition metals commonly used as catalysts in such reactions. Lithiation chemistry on the other hand is orthogonal to the phosphine and nitrogen functionality of the ligand.

The halogen lithium exchange reaction is almost instantaneous and goes to completion. However, the resulting lithiated intermediate is highly reactive, which can lead to deprotonation of other parts of the ligand (see the Supporting Information (SI) for details). These side reactions were mitigated by carrying out the reaction at low temperatures ($-108\text{ }^\circ\text{C}$) and adding the electrophile diethyl chlorophos-

Scheme 1. Retrosynthetic Pathway to a $\text{Ni}(\text{P}_2\text{N}_2)_2$ Complex Modified with a Surface Attachable Functional Group



Scheme 2. Synthesis of $[\text{Ni}(\text{P}^{\text{Ar}}\text{PO}_3\text{H}_2)_2\text{N}^{\text{Ph}}_2]_2$ [1] • HI

phate quickly after forming the lithium intermediate. Using this method, we were able to isolate the phosphonate substituted P_2N_2 ligand $\text{P}^{\text{Ar}}\text{PO}(\text{OEt})_2\text{N}^{\text{Ph}}_2$ (4) in 76% yield.

Ligand 4 was reacted with $[\text{Ni}(\text{MeCN})_6][\text{BF}_4]_2$ in acetonitrile yielding the corresponding $\text{Ni}(\text{P}_2\text{N}_2)_2$ complexes 5. The complex was structurally and spectroscopically characterized. The single crystal X-ray structure shows approximately trigonal bipyramidal geometries with the four phosphines and one MeCN solvent molecule coordinated to the nickel center similar to previously published $\text{Ni}(\text{P}_2\text{N}_2)_2$ complexes (Figure 2).^{5,21,22}

The cyclic voltammogram (CV) of 5 in acetonitrile shows two one-electron processes, characteristic for complexes of the type $[\text{Ni}(\text{P}_2\text{N}_2)_2]^{2+}$ (Figure S6). The reductions occur at

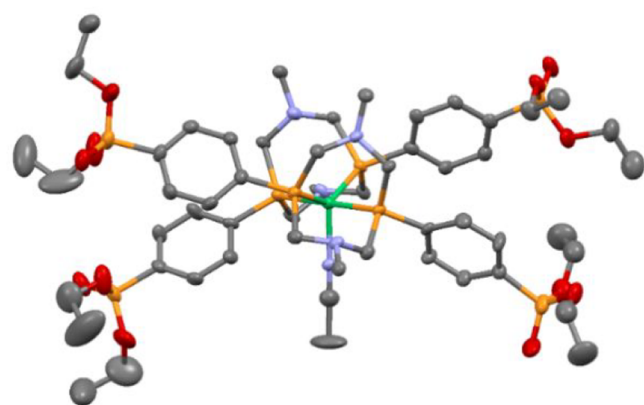
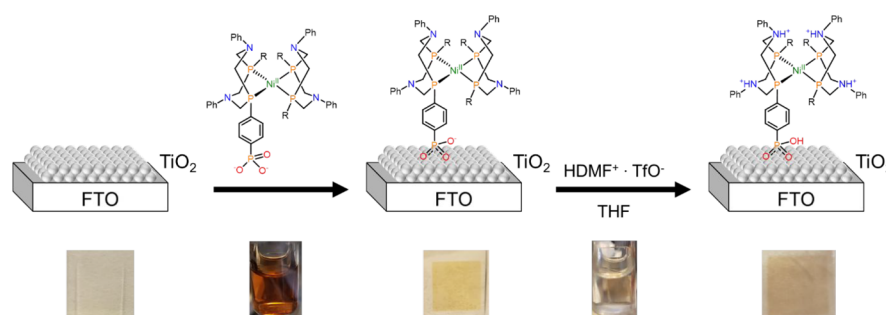


Figure 2. X-ray crystal structure of the dication of 5. Only *ipso* carbons of the nitrogen-bound phenyl rings are shown; counterions, and solvent are omitted for clarity.

-0.73 V ($\text{Ni}^{2+/+}$) and -0.89 V ($\text{Ni}^{+/0}$) vs $\text{Fc}^{+/0}$ and are fully reversible. This represents one of the least negative reduction potentials for the catalytically important second reduction reported to date. For comparison, $[\text{Ni}(\text{P}^{\text{Ph}}_2\text{N}^{\text{Ph}}_2)_2]^{2+}$ requires a potential over 100 mV more negative to reach the Ni^0 state. This positive shift in the CV of 5 is attributed to the strongly electron withdrawing nature of the phosphonate ester groups. Similar effects are observed for the complex with electron withdrawing trifluoromethyl phenyl substituted ligands.²³

To obtain a surface attachable catalyst, the phosphonate groups on 5 must be deprotected. We followed a modified procedure using TMS-I (trimethylsilyl iodide) to obtain the surface attachable catalyst 6. Interestingly, this treatment also leads to degradation of the BF_4^- counterion and liberation of the iodide that coordinates to the nickel center to form a stable five-coordinate complex (see SI for details). While not explicitly discussed, the same process is evident in previous reports with similar systems.^{10,16} After the removal of excess TMS-I, hydrolysis in MeOH, and precipitation with diethyl ether, 6 is isolated with a total of three iodides. Upon isolation, the complex is insoluble in common organic solvents, which limits the possibility of solution state studies, but the same low solubility makes it ideal as a heterogenized catalyst. It is slightly soluble in methanol acidified with excess triflic acid. In DMSO and basic H_2O , it will dissolve with slow degradation. However, if deprotonated in basic MeOH solution, an orange solution of 6' is formed. This color is consistent with a four-coordinate complex, indicating halogen dissociation due to the strong donating nature of the ligand in this deprotonated state (Scheme 2). These solutions are slightly air sensitive but are stable under an inert atmosphere and can be stored in a nitrogen filled glovebox for months without degradation.

Scheme 3. Schematic Representation of Surface Modification of Mesoporous TiO₂ Electrodes with 6' and Subsequent Protonation of the Attached Catalyst^a



^aAll R-substituents are phenylphosphonic acids and are omitted for clarity.

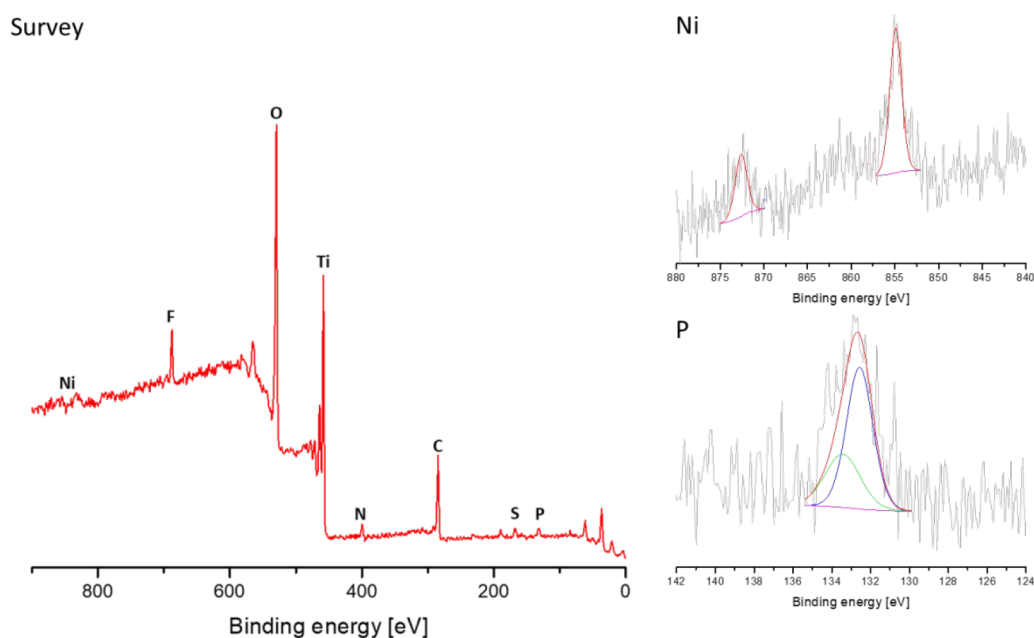


Figure 3. XPS spectra of mesoporous TiO₂/6 electrode after protonation with HDMF • TfO, as used in all electrochemical experiments. XPS peak positions (in eV): Ni (872.4, 854.9), F (688.5), N (399.8), S (165.9, 164.8), P (133.4, 132.6).

These solutions were used for NMR characterization of the complex and for its further utilization for surface modification.

Surface Modification and Characterization. As a support to heterogenize the catalyst, we chose mesoporous TiO₂. This material is well studied and commonly utilized to surface immobilize electrocatalysts in electro- and photocatalytic systems.^{10,12,24} Furthermore, there is comprehensive data¹² available for the attachment of P₂N₂ catalysts to this material, making it an excellent material to benchmark our new attachment strategy versus previously reported attachment through the amine moiety (7; Figure 1).¹² The electrodes were modified by soaking in methanolic solutions of the desired catalyst. Electrodes modified with 6' were found to be susceptible to degradation in air. To convert the catalyst back to its air stable fully protonated form, the electrodes were protonated with dimethylformamidium trifluoromethanesulfonate (HDMF • TfO). Both steps result in a color change of the electrode, indicative of the attachment and subsequent modification of the catalyst (Scheme 3). While the deprotonation and protonation step were not necessary for 7, they were still included in the procedure for consistency. At

this point, the electrodes were taken out of the glovebox for further study.

The catalyst loading was determined by desorption in 0.1 M NaOH and recording the UV–vis spectra of the solutions obtained following a previously reported procedure (Figure S7).¹² The loading before catalysis was determined to be 63 ± 1 nmol/cm² (6) and 60 ± 1 nmol/cm² (7), respectively, which is in agreement with previously reported data for similar systems.¹² This same procedure was followed to determine the surface loading of the electrodes after the controlled potential electrolysis (CPE) experiments. A catalyst retention of ~70% was observed for both systems supporting strong binding of the catalyst to the electrode. While the nature of electrodes modified with 7 is discussed in detail elsewhere,¹² we further confirmed the molecular integrity and surface binding of 6 with XPS and FTIR spectroscopy. XPS measurements of the electrodes were carried out using the air stable protonated form that was used in all electrochemical experiments. The survey scan (Figure 3) confirms the presence of Ni, F, O, Ti, N, C, S, and P, which is in agreement with the composition of the catalyst and support material. Two sharp peaks were observed at 872.4 and 854.9 eV, respectively, characteristic for

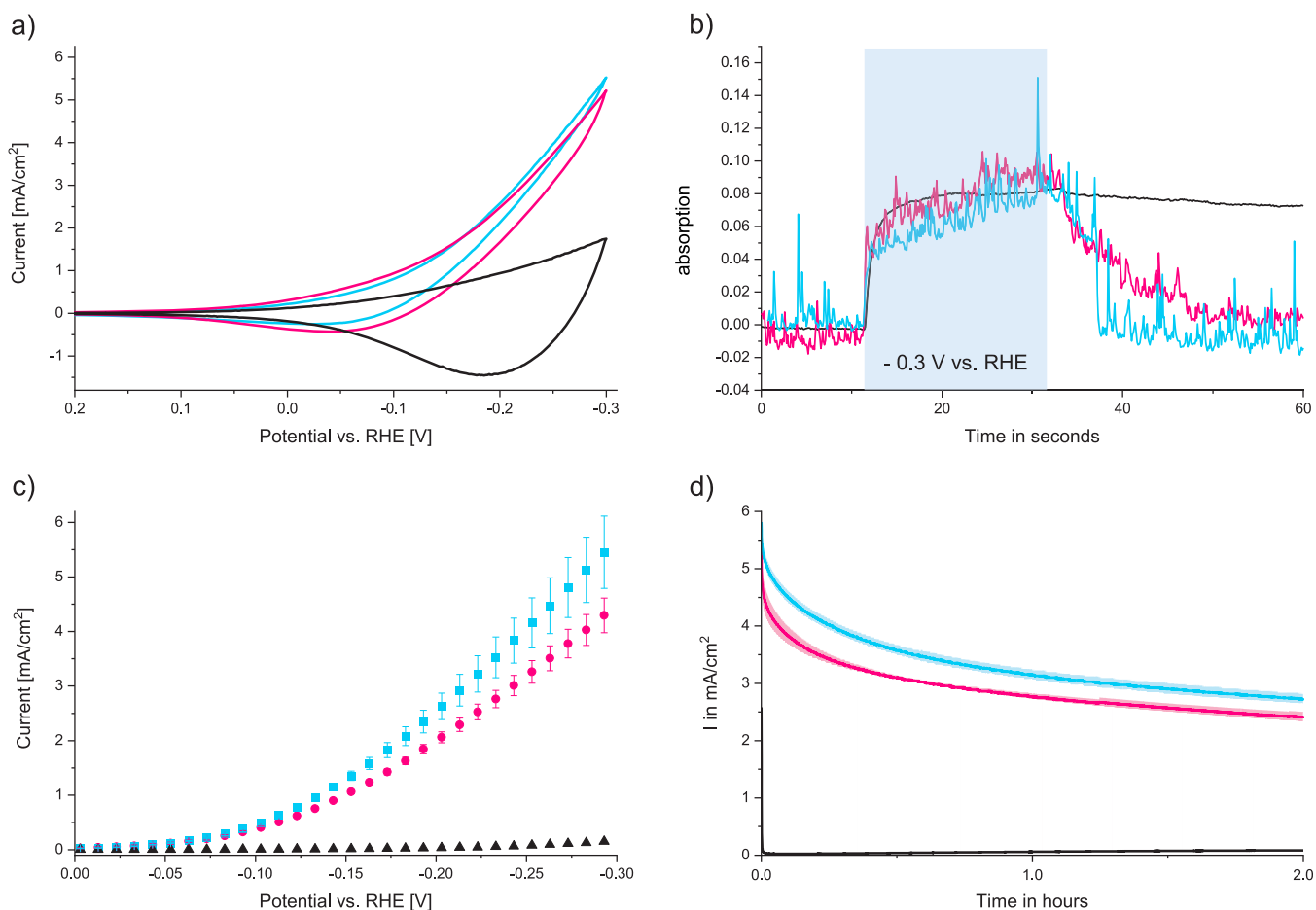


Figure 4. All experiments conducted in aqueous 0.5 M Na citrate buffer at pH 3. (a) CVs of TiO₂/6 (blue), TiO₂/7 (red), and TiO₂ (black) at 25 mV/s. (b) Kinetic trace of TiO₂/6 (blue), TiO₂/7 (red), and TiO₂ (black) electrodes' UV-vis absorption at 800 nm. The blue area indicates the duration of applied bias ($E = -0.3$ V vs RHE, 20 s). (c) SCP of TiO₂/6 (blue) TiO₂/7 (red), and TiO₂ (black); 10 mV steps at 5 s hold time with the end current of each step recorded. The data represents the average from three experiments for modified electrodes. The data for TiO₂ represents a single experiment. (d) CPE ($E = -0.3$ V vs RHE) of TiO₂/6 (blue), TiO₂/7 (red), and TiO₂ (black). Lines represent the average, and light areas represent the standard deviation from three experiments for modified electrodes. The data for TiO₂ represents a single experiment.

a Ni^{II} phosphine complex confirming that the complex is intact on the electrode. Furthermore, a peak at 132.9 eV confirms the presence of the phosphine and phosphonate groups of the ligand. The presence of F and S signals are in agreement with the presence of triflate ions from the treatment with HDMF • TfO.

Further evidence for the retention of molecular structure and covalent attachment of **6** to the TiO₂ was gained from attenuated total reflectance Fourier transform infrared (ATR-FTIR) spectroscopy. Figure S8 shows a comparison of FTIR spectra of powdered **5** and **6** and the surface-attached catalyst. All three spectra show strong peaks around 1500 and 1600 cm⁻¹ that are attributed to breathing modes of the aromatic substituents and a strong peak around 1140 cm⁻¹ that is attributed to a P–C stretch confirming the presence of the ligand on the surface. **5** exhibits a characteristic P=O stretch at 1244 cm⁻¹; for both powdered **6** and TiO₂/6, this feature is extremely weak, likely due to strong intermolecular interactions.²⁵ A characteristic P–OH stretch is observed for **6** at 989 cm⁻¹ that disappears after attachment. Instead, a new peak at 1050 cm⁻¹ emerges in agreement with the formation of a Ti–O–P bond, indicating covalent binding to the surface.²⁶

Effects of Attachment Moiety on Catalysis. To compare the new P-attached catalyst to the N-attached

version, we used HER in aqueous solution as the benchmark reaction. Screening of multiple electrolytes in aqueous solution showed that the nature of the electrolyte, its concentration as well as buffer capacity, has a major effect on catalysis. Figure S10 shows CPE performed with TiO₂/6 in different electrolytes. We found that a high electrolyte concentration with a large buffer capacity at low pH produced the greatest current density. One exception to this trend was 0.5 M HCl. With a pH of only 0.3, a high activity would be expected. Instead, it is comparable to pH 2 buffer systems. In agreement with literature reports,^{3,23} we attribute the reduced activity to the strong binding of chloride to the nickel center of the catalyst, suppressing catalysis. To maximize the influence from the pendent amine on catalysis, the reaction should be carried out at a pH close to the pK_a of the pendent amine. At higher pH, the amine will not be protonated sufficiently and therefore not contribute significantly to the catalytic activity. If the pH is much lower, direct protonation of the Ni by solution species will likely outcompete proton transfer through the amine, bypassing the “proton shuttle”. The amines of complex **7** were previously reported to have a pK_a ≈ 3.²⁷ We obtained the same value for the amines of **6** by acid base titration of the complex (see the SI for details). A system with excellent buffer

capacity at this pH was found in 0.5 M citric acid/sodium citrate buffer.

Cyclic voltammetry of 6- and 7-modified electrodes ($\text{TiO}_2/6$ and $\text{TiO}_2/7$) and unmodified TiO_2 in aqueous 0.5 M Na citrate buffer (pH 3) is shown in Figure 4 and exhibit catalytic activity for the modified electrodes. The CVs of $\text{TiO}_2/6$ and $\text{TiO}_2/7$ are both different in important details from the noncatalytic blank TiO_2 electrodes. The modified electrodes exhibit a catalytic wave with an onset potential around 0 V vs RHE. The shape of the electrochemical response is similar to that previously published for CVs of $\text{TiO}_2/7$.¹² The unmodified electrodes in contrast exhibit noncatalytic and reversible semiconductor charging, typical for TiO_2 .^{12,28}

The charging of the TiO_2 is accompanied by a reversible dark blue coloration of the electrode. The color change is due to an absorption band around 800 nm that can be attributed to a d–d transition of Ti^{3+} , which is formed when the TiO_2 conduction band is filled.^{12,28} This absorption can be leveraged to observe charge transfer kinetics from the TiO_2 to the catalyst.¹² Time resolved UV-spectroelectrochemistry (UV-SEC) illustrated in Figure 4 shows, that upon applying a potential ($E = -0.3$ V vs RHE, in aqueous citric acid buffer at pH 3), an immediate increase in absorption at 800 nm is observed for unmodified electrodes. The absorption persists even after bias is removed. This is consistent with the observation of a discharging current in the CV and suggests that the electrons populating the TiO_2 conduction band are not consumed by any subsequent Faradaic reactions. The electrodes modified with 6 or 7 also show a sharp increase in absorption when biased ($E = -0.3$ V vs RHE) under the same conditions. However, the initial absorption is lower than for unmodified electrodes. This reduced absorption suggests that there is efficient transfer of electrons from the TiO_2 to the catalyst, where they are consumed by the catalytic HER reaction. This limits the electron population in the conduction band. After bias was removed, we observe a rapid decrease in absorption for both modified electrodes. The P-modified ($t_{1/2} = 3$ s) electrode recovers twice as fast as the N-modified ($t_{1/2} = 6$ s). This suggests that the attachment through the phosphine moiety enhances catalysis on a molecular level. This observation is in stark contrast to the almost identical CVs for TiO_2 modified by 6 and 7. We hypothesize that the underlying semiconductor properties (charging and discharging of the TiO_2 conduction band) of the electrode material obscure the differences in catalytic activity in the CV experiments. To eliminate the background current of the TiO_2 and isolate the catalytic current in the system, we turned to scanning sampled current polarography (SCP). SCP allows the measurement of voltammograms of the catalytic response while eliminating the noncatalytic currents (capacitive, semiconductor charging). As for the CV experiments, SCP was conducted in aqueous 0.5 M Na citrate buffer at pH 3. We used a step potential of 10 mV with a 5 s hold time, which was sufficient to eliminate over 90% of the background current. $\text{TiO}_2/6$ electrodes showed a 27% higher current than $\text{TiO}_2/7$ electrodes averaged over three independent experiments for each material. Even taking the large standard deviation and a 5% difference in catalyst loading into account, the catalyst attached through the amine is marginally slower than its P-attached counterpart. This agrees with the observations from UV-SEC and the expectation that “pinning” the amines to the surface will lower the activity of the catalyst.

Hydrogen production was confirmed by CPE in aqueous 0.5 M Na citrate buffer at pH 3. CPE experiments for three electrodes ($\text{TiO}_2/6$ and $\text{TiO}_2/7$) were conducted with three independently prepared electrodes, each at a potential of $E = -0.3$ V vs RHE for 2 h, and the headspace was analyzed by gas chromatography. All electrodes tested showed continued HER over the 2 h period, and hydrogen was produced in quantitative Faradaic yield (Table S1). P-modified electrodes produced an average of 14% more hydrogen during this period compared to their N-attached counterparts. An unmodified TiO_2 electrode produced 2 orders of magnitude less H_2 , suggesting that TiO_2 in its native state does not significantly contribute to HER in this system. The 14% difference between the P- and N-modified is less than we expected given the widely discussed importance of the pendent amine.^{13,14} A commonly used parameter to benchmark molecular catalysts is the comparison of turnover numbers (TONs). However, using this metric is problematic, as the catalyst loading and activity can change over the course of the experiment. For our electrodes, we determined the loading before and after the CPE experiment, which leads to three distinct ways to calculate the TON. It can be calculated using the (i) initial loading, (ii) the final loading, (iii) or the average. (Table S1). If calculated assuming the initial catalyst loading, we obtained values of 1966 ± 54 for $\text{TiO}_2/6$ and 1802 ± 26 for $\text{TiO}_2/7$, respectively, corresponding to a 9% difference in TON for the 2 h CPE experiment. If calculated using postcatalysis loading, we obtained values of 2773 ± 380 for $\text{TiO}_2/6$ and 2433 ± 205 for $\text{TiO}_2/7$, respectively, corresponding to a 14% difference in TON. This difference between the two calculation methods and the increased error can be explained by the variation in postcatalysis loading. There is no positive correlation between postcatalysis loading and hydrogen produced. One would expect that electrodes that lose more catalyst also produce less hydrogen. This would lead to a similar TON between different experiments. For $\text{TiO}_2/6$ electrodes, a reverse trend was observed. The more current was passed, the lower the postcatalysis loading.

To understand this phenomenon, we must consider the underlying porous structure of the electrode and resulting implications on mass transport. Considering the high activity of the catalyst, a rapid consumption of the local proton supply is expected, even in highly buffered solutions as previously reported for other porous electrodes.²⁹ Small differences in electrolysis conditions can lead to slightly higher catalytic rates, leading to an increased local pH that results in a loss of catalyst (phosphonates are known to desorb under basic conditions).³⁰ This would explain why electrodes that produce the most hydrogen also lose the most catalyst.

UV-SEC allows for qualitative insight into the rate of substrate depletion from the electrode. After the initial jump in absorption (TiO_2 conduction at band 800 nm) upon biasing the electrode, we observed a gradual increase in absorption that continued until the bias was removed. We attribute this gradual increase to a slowing of the rate of catalysis caused by a pH change in the local surface microenvironment, allowing the TiO_2 conduction band to be further populated by carriers. Further evidence suggesting that we are indeed observing a temporary increase in local pH induced by catalysis can be found in the overproportionally large current drop compared to the effective loss of catalyst. If this drop is due to a temporary change, the measured current should recover after the bias is removed and the system is given time to equilibrate.

To test this hypothesis, we conducted a series of 5 min CPE experiments with sequential 5 min equilibrations between electrolyses. A recovery of over 95% of the initial current was observed (Figure S11). This time scale and previous SCP experiments suggest that the current drop cannot be explained by non-Faradaic processes (capacitive and semiconductor charging). This leads us to the conclusion that the main cause of loss of catalytic activity over time can be attributed to a change in local surface environment caused by substrate depletion and a steady state increase in local pH. However, further studies are necessary to directly observe a pH increase in our system, and other explanations for the current drop, like a temporary catalyst deactivation, should also be considered.

Together, these results indicate that the catalyst attachment through the phosphine moiety (TiO₂/6) yields a slightly more active electrocatalyst material, but the effect relative to amine attachment (TiO₂/7) is less than expected. While “pinning down” the amine impedes catalysis on a molecular level, the effect on a macroscopic level may be small. For example, the overall limitations in diffusion through the porous support material and fundamental differences in mass transport in homogeneous and heterogeneous electrocatalyst systems may be more important. Most of the early studies of Ni(P₂N₂)₂ were carried out in aprotic organic solvents such as acetonitrile.^{5,21} In contrast, the system described here operates in an aqueous environment with an abundance of highly mobile protons, where the beneficial effect of the pendent amine proton relay may not be as important as it is in nonaqueous solvents. Literature reports show that the addition of water to organic solvents or ionic liquids can dramatically enhance the turnover frequency (TOF) of Ni(P₂N₂)₂.^{31,32} But most importantly, the TOFs of the heterogenized catalysts are nowhere near the extraordinary levels reported for homogeneous Ni(P₂N₂)₂ HER catalysts.^{23,33} Thus, it is likely that much simpler Ni-phosphine complexes without pendent amines can achieve comparable performance in a surface-immobilized system with a carefully designed microenvironment at the electrode interface.

CONCLUSION

While there are many derivatives of Ni(P₂N₂)₂ catalysts with different functional groups on the pendent base amine groups, there is only a very limited library of reported P₂N₂s with variation in substituents on the phosphine. We presented a versatile new synthetic strategy to overcome limitations of previous approaches utilizing the 4-BrP₂N₂ ligand as a platform that can be easily converted into other functional groups. This approach enabled us to synthesize [Ni(P^{Ar}PO(OEt)₂N^{Ph})₂][BF₄]₂ and [INi(P^{Ar}PO₃H₂N^{Ph})₂][I] • HI. This represents not only the first reported P₂N₂ ligand that has a reactive functional group on the phosphine but also the first P₂N₂ complex that was successfully attached to an electrode surface without utilizing the pendent amine. A mesoporous TiO₂ electrode modified with the catalyst sustains HER in water at mild pH and low overpotential. The catalytic performance for HER was used as a benchmark for direct comparison of the phosphine anchored catalyst 6 to the previously reported complex 7 anchored through the amine moiety. Electrodes prepared with 6 showed higher activity in UV-SEC and SCP compared to 7. This is further confirmed by CPE, with 6 showing a 9–14% increase in activity for HER over 7. However, these experiments also show the importance of the microenvironment on the electrode surface. The combination

of results from the experiments reported here indicate that the catalyst attachment through the phosphine moiety yields a slightly more active electrocatalyst, but the effect is smaller than expected. While “pinning down” the amine impedes catalysis on a molecular level, the macroscopic effects of the electrocatalyst material and environment that include mass transport through the porous support and an abundance of protons in the aqueous solution appear to determine performance. Finally, we illustrated the importance of direct comparative studies for understanding the nature of heterogenized molecular electrocatalysts and the many parameters that can sometimes influence activities unpredictably.

EXPERIMENTAL SECTION

Materials and Methods. ¹³C NMR spectra were recorded on a Varian 500 MHz spectrometer. ¹H, ³¹P, and ¹⁹F spectra were recorded on a Bruker 300 MHz spectrometer. The ¹³C and ¹H chemical shifts are referenced to deuterated solvent peaks (δTMS = 0), and ³¹P spectra are referenced to 85% H₃PO₄. ATR-FTIR spectra were recorded on a Bruker Alpha II. Microanalyses were performed by NuMega Resonance Laboratories, San Diego, CA, for C, H, and N. XPS was performed on a SSF-Kratos AXIS-SUPRA. Mass spectrometry was performed on a Micromass Quattro Ultima. High resolution mass spectrometry was performed on an Agilent 6230 Accurate-Mass TOFMS. UV–vis spectra were collected on a Shimadzu UV-3600. Solvents were received from Fisher Scientific and were dried on a custom solvent system (degassed with argon and dried over alumina columns) and stored over 3 Å sieves. Deuterated solvents were obtained from Cambridge Isotope Laboratories. [Ni(CH₃CN)₆][BF₄]₂³⁴ and 7¹⁵ were synthesized following previously reported procedures; aniline and triethylamine were distilled from CaH₂ and stored over 3 Å sieves in a N₂ filled glovebox. All other reagents were obtained from commercial sources and used without further purification. Reactions were performed using standard Schlenk line and glove box techniques under an atmosphere of nitrogen. Flash column chromatography was performed on a Teledyneisco CombiFlash Rf200 using SiO₂ loaded columns. Mesoporous TiO₂ electrodes were obtained from Solaronix and cut to fit the electrochemical cell. They were brought into a N₂ filled glovebox, where all surface modification was carried out.

X-ray Crystallography. Single crystal X-ray data was collected on a Bruker Kappa APEX-II CCD diffractometer equipped with Mo Kα radiation (λ = 0.71073 Å). The crystals were mounted on a CryoLoop with paratone oil, and data were collected under a nitrogen gas stream at 100 K using ω and φ scans. Data were integrated using the Bruker SAINT software program and scaled using the software program. All structures were solved via direct methods with SHELXS³⁵ and refined by full-matrix least-squares procedures using SHELXL21 within the Olex2 small-molecule solution, refinement, and analysis software package.³⁶ All non-hydrogen atoms were refined anisotropically by full-matrix least-squares (SHELXL-97). All hydrogen atoms were placed using a riding model. Their positions were constrained relative to their parent atom using the appropriate HFIX command. Crystallographic data, structure refinement parameters, and additional notes on structure refinement are summarized in the SI.

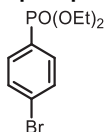
Electrochemistry. Electrochemical experiments with an immobilized catalyst were carried out in a custom build five-port 90 mL glass cell. The modified electrode was the working electrode, a graphite rode separated from the solution by a porous glass frit was used as the counter electrode, and an aqueous Ag/AgCl (3 M NaCl) electrode separated from the solution by a Vycor tip was used as the reference. The working, counter, and reference electrodes occupied one ground glass joint each. The remaining two ports were sealed with rubber septa, allowing for gas purging of the cell. The potential was controlled by a BASi Epsilon potentiostat. The solution was stirred during experiments. Homogenous electrochemical experiments were carried out in acetonitrile solution in an oven-dried 20 mL vial with [nBu₄N][PF₆] as the supporting electrolyte. A glassy carbon rod was

used as the counter electrode, and a silver wire separated from the solution by a Vycor tip was used as a pseudoreference electrode. All potentials are referenced versus an internal ferrocene standard.

UV Spectroelectrochemistry. UV-SEC was performed in a custom build UV-SEC cell. The cell was operated in transmission mode with the electrode masked to expose a surface area of 0.36 mm². Catalytic UV-SEC experiments were carried out in aqueous Na citrate buffer (pH 3.0, 0.5 M). The potential was controlled by a BASi Epsilon potentiostat, and spectra were collected on a Shimadzu UV-3600.

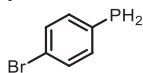
Surface Modification. Mesoporous TiO₂ on fluorine doped tin oxide (FTO) electrodes were purchased from Solaronix and cut to size to fit the electrochemical cell. The TiO₂ layer is made from 15 to 20 nm particles with a physical area of 6 by 6 mm and 12 μm thickness (as determined by SEM; Figure S12). The electrodes were modified by soaking in methanolic solutions (6', 1 mM; 7, 0.1 mM) of the desired catalyst and 10 equiv of triethylamine (NEt₃) for 20 h. The concentration of 7 compared to 6' was adjusted to maintain the same catalyst loading despite different adsorption kinetics. After being rinsed with MeOH, the electrodes were soaked in MeOH for 1 h to remove any unattached catalyst. In this form, the electrodes modified with 6' are susceptible to degradation in air. To convert the catalyst back to the air stable fully protonated form, the electrodes were soaked in dimethylformamidium trifluoromethanesulfonate (HDMF • TfO) (10 mM in THF) solution for 10 min, rinsed with THF, and soaked in THF for 1 h.

Diethyl (4-Bromophenyl)phosphonate (1).



In a 1 L Schlenk flask, 1,4-dibromobenzene (10.00 g, 42.4 mmol, 1.0 equiv) was dissolved in dry degassed Et₂O (450 mL). At -78 °C, *n*-butyl-lithium (29.2 mL, 46.6 mmol, 1.1 equiv of 1.6 M in hexane) was added dropwise, and the solution was stirred at -78 °C for 1 h. The solution was then added dropwise via a cannula to a stirred solution of diethyl chlorophosphate (15.3 mL, 106.0 mmol, 2.5 equiv) in Et₂O (75 mL) at -78 °C. After the addition was completed, the solution was stirred for 1 h at -78 °C and then warmed to room temperature over 1.5 h. The reaction was quenched with water and extracted with DCM. After the solvent was evaporated, the residue was purified by flash column chromatography (hexane to ethyl acetate) to obtain the title compound as a colorless oil (10.85 g, 37.02 mmol, 87%). NMR spectroscopic data were consistent with literature values.¹⁹

(4-Bromophenyl)phosphane (2).



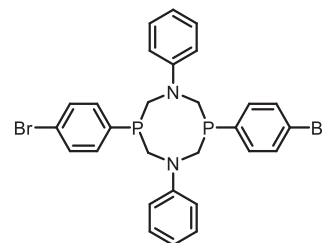
A solution of diethyl (4-bromophenyl)phosphonate (2.00 g, 6.82 mmol, 1.0 equiv) in dry Et₂O (10 mL) was degassed and added dropwise to a suspension of LiAlH₄ (647 mg, 17.06 mmol, 2.5 equiv) in Et₂O (20 mL) at 0 °C. Gas production was observed. After the green suspension was stirred for 1.5 h at 0 °C, it was quenched by the addition of degassed water (1.7 mL), resulting in a violent reaction, with large quantities of gas produced. The off-white suspension was warmed to room temperature, and the solvent was removed under reduced pressure on a Schlenk line. The residue was extracted with pentane (4 × 30 mL), and the solvent was evaporated under reduced pressure at the Schlenk line. The title compound (*extremely toxic with a very strong unpleasant odor*) was obtained as a white solid (605 mg, 3.02 mmol, 47%, 90% pure by NMR) and used without further purification.

¹H NMR (300 MHz, CDCl₃) δ/ppm 7.50–7.20 (m, 4H, Ar), 3.93 (d, *J* = 202.3 Hz, 2H, PH₂).

¹³C {¹H} NMR (126 MHz, CDCl₃) δ/ppm 136.35 (d, *J* = 15.7 Hz, C3), 131.65 (d, *J* = 6.0 Hz, C2), 127.68 (d, *J* = 8.7 Hz, C4), 122.87 (s, C1).

³¹P{¹H} NMR (121 MHz, CDCl₃) δ/ppm +123.1 (s).

P^{Ar}Br₂N^{Ph}₂ (3).



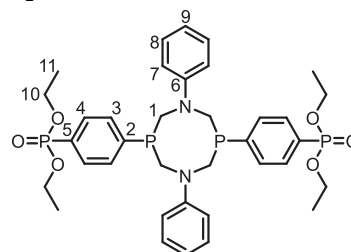
In a 500 mL, two-neck, round-bottom flask with a reflux condenser, (4-bromophenyl)phosphane (3.49 g, 16.6 mmol, 1.0 eq, 90%) and *para*-formaldehyde (998 mg, 33 mmol, 2.0 equiv) were mixed in dry degassed EtOH (150 mL) and heated to reflux for 17 h until a clear solution was formed. Then, aniline (1.5 mL, 1.55 g, 17 mmol, 1.0 equiv) was added, and the solution was heated to reflux for 1 day, during which a white precipitate was formed. After the solution was cooled to room temperature, the solid was filtered off via a cannula under N₂ and washed with EtOH. After drying under vacuum, the title compound was obtained as a white solid (3.0 g, 4.90 mmol, 59%).

¹H NMR (300 MHz, CD₂Cl₂) δ 7.67 (dd, *J* = 21.9, 8.5 Hz, 4H, H^{ArP3}), 7.54–7.46 (m, 4H, H^{ArP2}), 7.20 (t, *J* = 7.9 Hz, 4H, H^{ArN3}), 6.76–6.66 (m, 6H, H^{ArN2, ArN4}), 4.49–3.95 (m, 8H, H^{NCH2P}).

³¹P{¹H} NMR (121 MHz, CD₂Cl₂) δ/ppm 51.0.

IR (ATR) ν_{max} [cm⁻¹]: 3257 (wbr), 3088 (w), 3036 (w), 2959 (w), 2873 (w), 1902 (w), 1591 (s), 1498 (s), 1474 (m), 1450 (w), 1425 (w), 1374 (m), 1343 (w), 1249 (m), 1230 (w), 1206 (m), 1161 (w), 1145 (w), 1108 (w), 1091 (w), 1065 (m), 1036 (w), 1004 (m), 991 (w), 955 (w), 934 (w), 908 (w), 877 (w), 859 (w), 806 (s), 738 (s), 720 (m), 680 (s), 601 (w), 511 (m), 476 (w).

HR-ESI-MS: *m/z* calcd for [M + H]⁺ 611.0011 (found) 611.0007. P^{Ar}PO(OEt)₂N^{Ph}₂ (4).



A saturated solution of P^{Ar}Br₂N^{Ph}₂ (500 mg, 816.61 μmol, 1.0 equiv) in dry degassed THF (500 mL) was cooled to -108 °C in a glovebox. *n*-Butyl-lithium (1.12 mL, 1.6 M in hexanes, 1.80 mmol, 2.2 equiv) was added, and the solution was cooled back to -108 °C (4 min). Diethyl chlorophosphate (590 μL, 4.01 mmol, 5.0 equiv) was added, and the solution was warmed to room temperature over 3 h. The solvent was removed under vacuum, and the crude was purified by flash column chromatography (SiO₂ treated with a 2% solution of TEA in DCM and washed with DCM, DCM to DCM/5% MeOH). The title compound was isolated as a white solid (448 mg, 617 μmol, 76%). This ligand is moderately air stable and can be handled out of the glovebox for short periods (1 h) without significant degradation, simplifying the purification by flash column chromatography.

¹H NMR (300 MHz, CDCl₃) δ/ppm 7.90 (dd, *J* = 13.1, 7.8 Hz, 4H, H¹), 7.74–7.65 (m, 4H, H³), 7.22 (dd, *J* = 8.4, 7.7 Hz, 4H, H⁸), 6.78–6.67 (m, 6H, H⁷, H⁹), 4.50 (t, *J* = 14.0 Hz, 4H, H¹), 4.28–4.10 (m, 8H, H¹⁰), 4.02 (dd, *J* = 15.2, 4.6 Hz, 4H, H¹), 1.37 (t, *J* = 7.1 Hz, 12H, H¹¹).

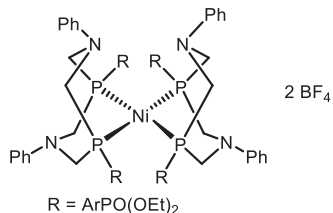
¹³C{¹H} NMR (126 MHz, CDCl₃) δ/ppm 145.16 (s, C⁶), (C²), 132.86–132.39 (m, C³), 132.27–131.83 (m, C⁴), 129.77 (d, *J* = 188.3 Hz, C⁵), 129.37 (s, C⁸), 117.46 (s, C⁹), 112.91 (s, C⁷), 62.46 c (d, *J* = 5.5 Hz, C¹⁰), 57.97 (d, *J* = 17.4 Hz, C¹), 16.53 (d, *J* = 6.5 Hz, C¹¹).

³¹P{¹H} NMR (121 MHz, CDCl₃) δ/ppm 17.78 (s, PO(OEt)₂), -49.44 (s, NCH₂P).

IR (ATR) ν_{max} [cm⁻¹]: 3064 (w), 2982 (m), 2934 (w), 2902 (w), 1590 (s), 1500 (s), 1472 (w), 1380 (w), 1368 (s), 1343 (m), 1244

(s), 1214 (m), 1148 (w), 1135 (m), 1098 (w), 1014 (s), 943 (s), 893 (w), 874 (m), 795 (m), 773 (m), 741 (s), 684 (s), 648 (w), 585 (s), 537 (s), 447 (w).

HR-ESI-MS: m/z calcd for $[M + H]^+$ 727.2379 (found) 727.2372. $[\text{Ni}(\text{P}^{\text{ArPO}(\text{OEt})_2}_2\text{N}^{\text{Ph}}_2)_2] [\text{BF}_4]_2$ (**5**).



To a suspension of $\text{P}^{\text{ArPO}(\text{OEt})_2}_2\text{N}^{\text{Ph}}_2$ (387 mg, 532.57 μmol , 2.0 equiv) in MeCN (5 mL), a solution of $[\text{Ni}(\text{MeCN})_6] [\text{BF}_4]_2$ (127 mg, 266.28 μmol , 1.0 equiv) in MeCN (5 mL) was added. After the mixture was stirred at room temperature for 1 h, the solvent was removed under vacuum, and the residue was redissolved in minimal MeCN. The addition of Et_2O led to a precipitate that was filtered off and dried under vacuum to yield the title compound as a dark red solid (227 mg, 135 μmol , 98%). Single X-ray quality crystals were grown by vapor diffusion of Et_2O into a MeCN solution of the complex.

^1H NMR (300 MHz, CD_3CN) δ/ppm 7.56–7.38 (m, 24H, $\text{H}^{\text{ArP}}, \text{N}^3$), 7.29 (d, $J = 8.1$ Hz, 8H, $\text{H}^{\text{N}2}$), 7.16 (t, $J = 7.2$ Hz, 4H, $\text{H}^{\text{N}4}$), 4.30–3.88 (m, 32H, $\text{H}^{\text{NCH}_2\text{P}}, \text{PCH}_2\text{Me}$), 1.38 (dd, $J = 11.4, 6.9$ Hz, 24H, H^{Me}).

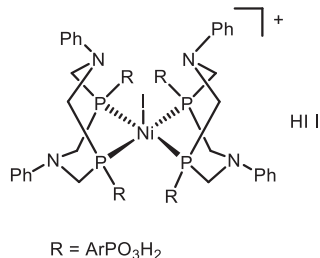
$^{13}\text{C}\{^1\text{H}\}$ NMR (126 MHz, CD_3CN) δ 152.1–152.0 (m, $\text{C}^{\text{P}4}, \text{N}1$), 133.8 (d, $J = 186.4$ Hz, $\text{C}^{\text{P}1}$), 132.8 (d, $J = 9.5$ Hz, $\text{C}^{\text{P}3}$), 132.1 (d, $J = 14.4$ Hz, $\text{C}^{\text{P}2}$), 130.5 (s, $\text{C}^{\text{N}3}$), 124.3 (s, $\text{C}^{\text{N}4}$), 120.6 (s, $\text{C}^{\text{N}2}$), 63.4 (t, $J_{\text{CC}} = 5.3$ Hz, $\text{C}^{\text{CH}_2\text{Me}}$), 52.3 (d, $J = 911.5$ Hz, $\text{C}^{\text{NCH}_2\text{P}}$), 16.6 (d, $J = 4.8$ Hz, C^{Me}).

$^{31}\text{P}\{^1\text{H}\}$ NMR (121 MHz, CD_3CN) δ/ppm 16.6 (s, $\text{P}^{\text{O}(\text{OEt})_2}$), 6.3 (s, $\text{P}^{\text{NCH}_2\text{P}}$).

HR-ESI-MS: m/z calcd for $[M + \text{Cl}^- - 2[\text{BF}_4]^+]$ 1545.3655 (found) 1545.3666; $[M + \text{CN}^- - 2[\text{BF}_4]^+]$ 1536.3997 (found) 1536.4027. (Isotope patterns match for both molecules. The presence of Cl^- and CN^- is an artifact of the technique and not present in the isolated compound).

IR (ATR) ν_{max} [cm^{-1}]: 3060 (w), 2983 (m), 2935 (w), 2908 (w), 1595 (s), 1494 (s), 1442 (w), 1420 (w), 1387 (m), 1246 (s), 1191 (m), 1162 (w), 1136 (m), 1044 (w), 1011(s), 967 (s), 886 (w), 793 (w), 759 (w), 694 (w), 589 (s), 540 (m).

$[\text{Ni}(\text{P}^{\text{ArPO}_3\text{H}_2}_2\text{N}^{\text{Ph}}_2)_2] [\text{I}] \cdot \text{HI}$ (**6**).



To a solution of $[\text{Ni}(\text{P}^{\text{ArPO}(\text{OEt})_2}_2\text{N}^{\text{Ph}}_2)_2] [\text{BF}_4]_2$ (250 mg, 145 μmol , 1.0 equiv) in dry degassed DCM (15 mL), TMS-I (270 μL , 1.88 mmol, 13.0 equiv) was added. The solution turns dark purple immediately and was stirred at room temperature for 5 h before the solvent was removed under vacuum. To the residue, dry degassed MeOH (15 mL) was added, and the resulting suspension was stirred overnight. The solvent was reduced to about one-third, and Et_2O (25 mL) was added and stirred for 30 min. The resulting precipitate was filtered, washed with Et_2O , and dried under vacuum, yielding the title compound as a dark purple solid (187 mg, 112 μmol , 77%) (NMRs recorded of deprotonated species; 10 equiv of NEt_3 added).

^1H NMR (300 MHz, CD_3OD) δ/ppm 8.18–6.30 (m, 36H, H^{Ar}), 4.77–3.42 (m, 16, $\text{H}^{\text{NCH}_2\text{P}}$).

$^{31}\text{P}\{^1\text{H}\}$ NMR (121 MHz, CDCl_3) δ/ppm 12.7 (s, P^{NCH_2}), 10.1 (s, $\text{P}^{\text{O}(\text{OEt})_2}$).

IR (ATR) ν_{max} [cm^{-1}]: 2857 (br), 1594 (s), 1492 (s), 1383 (m), 1190 (s), 1140 (s), 989 (m), 921 (m), 882 (m), 814 (w), 747 (s), 692 (w), 569 (s), 531 (s).

Anal. Calcd for $\text{C}_{56}\text{H}_{60}\text{I}_2\text{N}_4\text{NiO}_{12}\text{P}_8 \cdot \text{HI} \cdot 2\text{H}_2\text{O}$: C, 39.44; H, 3.84; N, 3.29. Found: C, 39.36; H, 4.07; N, 3.20.

■ ASSOCIATED CONTENT

Supporting Information

The Supporting Information is available free of charge at <https://pubs.acs.org/doi/10.1021/acs.inorgchem.0c01669>.

NMR quenching studies of Li-intermediate, degradation of BF_4 by TMS-I during deprotection reaction, solution CV of $[\text{Ni}(\text{P}^{\text{Ph}}_2\text{N}^{\text{Ph}}_2)_2]^{2+}$ and **5**, IR spectra, UV–vis spectra of desorbed catalyst, pH titration of **6**, heterogenous electrochemistry data, SEM data, NMR spectra, crystallographic data (PDF)

Accession Codes

CCDC 1985396 contains the supplementary crystallographic data for this paper. These data can be obtained free of charge via www.ccdc.cam.ac.uk/data_request/cif, or by emailing data_request@ccdc.cam.ac.uk, or by contacting The Cambridge Crystallographic Data Centre, 12 Union Road, Cambridge CB2 1EZ, UK; fax: +44 1223 336033.

■ AUTHOR INFORMATION

Corresponding Author

Clifford P. Kubiak – Department of Chemistry and Biochemistry, University of California, San Diego, La Jolla, California 92093-0358, United States; orcid.org/0000-0003-2186-488X; Email: ckubiak@ucsd.edu

Authors

Felix M. Brunner – Department of Chemistry and Biochemistry, University of California, San Diego, La Jolla, California 92093-0358, United States

Michael L. Neville – Department of Chemistry and Biochemistry, University of California, San Diego, La Jolla, California 92093-0358, United States

Complete contact information is available at:

<https://pubs.acs.org/10.1021/acs.inorgchem.0c01669>

Notes

The authors declare no competing financial interest.

■ ACKNOWLEDGMENTS

This work was supported by the Air Force Office of Scientific Research under Award No. FA9550-17-0198. We acknowledge the UCSD Molecular Mass Spectrometry Facility for HRMS sample analysis, Dr. Po Ling Cheung for recording SEM images, and Dr. Ich Tran for the XPS measurements performed at the UC Irvine Materials Research Institute (IMRI) using instrumentation funded in part by the National Science Foundation Major Research Instrumentation Program under grant no. CHE-1338173.

■ REFERENCES

- Stubbs, J. M.; Hazlehurst, R. J.; Boyle, P. D.; Blacquiere, J. M. Catalytic acceptorless dehydrogenation of amines with $\text{Ru}(\text{P}^{\text{R}2}\text{N}^{\text{R}2})$ and $\text{Ru}(\text{dppp})$ complexes. *Organometallics* **2017**, *36* (9), 1692–1698.
- Weiss, C. J.; Das, P.; Miller, D. L.; Helm, M. L.; Appel, A. M. Catalytic Oxidation of Alcohol via Nickel Phosphine Complexes with Pendant Amines. *ACS Catal.* **2014**, *4* (9), 2951–2958.

- (3) Seu, C. S.; Appel, A. M.; Doud, M. D.; DuBois, D. L.; Kubiak, C. P. Formate oxidation via β -deprotonation in $[\text{Ni}(\text{P}^{\text{R}2}\text{N}^{\text{R}2})_2(\text{CH}_3\text{CN})]^{2+}$ complexes. *Energy Environ. Sci.* **2012**, *5* (4), 6480.
- (4) Roy, S.; Sharma, B.; Pecaut, J.; Simon, P.; Fontecave, M.; Tran, P. D.; Derat, E.; Artero, V. Molecular Cobalt Complexes with Pendant Amines for Selective Electrocatalytic Reduction of Carbon Dioxide to Formic Acid. *J. Am. Chem. Soc.* **2017**, *139* (10), 3685–3696.
- (5) Wilson, A. D.; Newell, R. H.; McNevin, M. J.; Muckerman, J. T.; Rakowski DuBois, M.; DuBois, D. L. Hydrogen Oxidation and Production Using Nickel-Based Molecular Catalysts with Positioned Proton Relays. *J. Am. Chem. Soc.* **2006**, *128* (1), 358–366.
- (6) Le Goff, A.; Artero, V.; Jousselmé, B.; Tran, P. D.; Guillet, N.; Métayé, R.; Fihri, A.; Palacin, S.; Fontecave, M. From Hydrogenases to Noble Metal-Free Catalytic Nanomaterials for H_2 Production and Uptake. *Science* **2009**, *326* (5958), 1384–1387.
- (7) Moore, G. F.; Sharp, I. D. A Noble-Metal-Free Hydrogen Evolution Catalyst Grafted to Visible Light-Absorbing Semiconductors. *J. Phys. Chem. Lett.* **2013**, *4* (4), 568–72.
- (8) Das, A. K.; Engelhard, M. H.; Lense, S.; Roberts, J. A. S.; Bullock, R. M. Covalent attachment of diphosphine ligands to glassy carbon electrodes via Cu-catalyzed alkyne-azide cycloaddition. Metallation with Ni(II). *Dalton Trans.* **2015**, *44* (27), 12225–12233.
- (9) Rodriguez-Maciá, P.; Dutta, A.; Lubitz, W.; Shaw, W. J.; Rüdiger, O. Direct Comparison of the Performance of a Bio-inspired Synthetic Nickel Catalyst and a $[\text{NiFe}]$ -Hydrogenase, Both Covalently Attached to Electrodes. *Angew. Chem., Int. Ed.* **2015**, *54* (42), 12303–12307.
- (10) Shan, B.; Das, A. K.; Marquard, S.; Farnum, B. H.; Wang, D.; Bullock, R. M.; Meyer, T. J. Photogeneration of hydrogen from water by a robust dye-sensitized photocathode. *Energy Environ. Sci.* **2016**, *9* (12), 3693–3697.
- (11) Huan, T. N.; Jane, R. T.; Benayad, A.; Guetaz, L.; Tran, P. D.; Artero, V. Bio-inspired noble metal-free nanomaterials approaching platinum performances for H_2 evolution and uptake. *Energy Environ. Sci.* **2016**, *9* (3), 940–947.
- (12) Rosser, T. E.; Gross, M. A.; Lai, Y.-H.; Reisner, E. Precious-metal free photoelectrochemical water splitting with immobilised molecular Ni and Fe redox catalysts. *Chem. Sci.* **2016**, *7* (7), 4024–4035.
- (13) Appel, A. M.; Pool, D. H.; O'Hagan, M.; Shaw, W. J.; Yang, J. Y.; Rakowski DuBois, M.; DuBois, D. L.; Bullock, R. M. $[\text{Ni}(\text{P}^{\text{Ph}2}\text{N}^{\text{Bn}2})_2(\text{CH}_3\text{CN})]^{2+}$ as an Electrocatalyst for H_2 Production: Dependence on Acid Strength and Isomer Distribution. *ACS Catal.* **2011**, *1* (7), 777–785.
- (14) Fernandez, L. E.; Horvath, S.; Hammes-Schiffer, S. Theoretical Analysis of the Sequential Proton-Coupled Electron Transfer Mechanisms for H_2 Oxidation and Production Pathways Catalyzed by Nickel Molecular Electrocatalysts. *J. Phys. Chem. C* **2012**, *116* (4), 3171–3180.
- (15) Gross, M. A.; Reynal, A.; Durrant, J. R.; Reisner, E. Versatile photocatalytic systems for H_2 generation in water based on an efficient DuBois-type nickel catalyst. *J. Am. Chem. Soc.* **2014**, *136* (1), 356–66.
- (16) Gross, M. A.; Reynal, A.; Durrant, J. R.; Reisner, E. Versatile photocatalytic systems for H_2 generation in water based on an efficient DuBois-type nickel catalyst. *J. Am. Chem. Soc.* **2014**, *136* (1), 356–66.
- (17) Bonnaventure, I.; Charette, A. B. Probing the Importance of the Hemilabile Site of Bis(phosphine) Monoxide Ligands in the Copper-Catalyzed Addition of Diethylzinc to N-Phosphinoylimines: Discovery of New Effective Chiral Ligands. *J. Org. Chem.* **2008**, *73* (16), 6330–6340.
- (18) Brown, H. C.; Krishnamurthy, S. Selective reductions. XIV. Fast reaction of aryl bromides and iodides with lithium aluminum hydride in tetrahydrofuran. Simple convenient procedure for the hydrogenolysis of aryl bromides and iodides. *J. Org. Chem.* **1969**, *34* (12), 3918–3923.
- (19) Edder, C.; Fréchet, J. M. J. Synthesis of Bridged Oligothiophenes: Toward a New Class of Thiophene-Based Electroactive Surfactants. *Org. Lett.* **2003**, *5* (11), 1879–1882.
- (20) Maerkl, V. G.; Jin, G. Y.; Schoerner, C. 1,5-Diaza-3,7-diphosphacyclooctanes. *Tetrahedron Lett.* **1980**, *21* (15), 1409.
- (21) Kilgore, U. J.; Roberts, J. A. S.; Pool, D. H.; Appel, A. M.; Stewart, M. P.; DuBois, M. R.; Dougherty, W. G.; Kassel, W. S.; Bullock, R. M.; DuBois, D. L. $[\text{Ni}(\text{P}^{\text{Ph}2}\text{N}^{\text{C}6\text{H}4\times 2})_2]^{2+}$ Complexes as Electrocatalysts for H_2 Production: Effect of Substituents, Acids, and Water on Catalytic Rates. *J. Am. Chem. Soc.* **2011**, *133* (15), 5861–5872.
- (22) Galan, B. R.; Schoeffel, J.; Linehan, J. C.; Seu, C.; Appel, A. M.; Roberts, J. A. S.; Helm, M. L.; Kilgore, U. J.; Yang, J. Y.; DuBois, D. L.; Kubiak, C. P. Electrocatalytic oxidation of formate by $\text{Ni}(\text{P}(\text{R})-2\text{N}(\text{R}')_2)(\text{CH}_3\text{CN})_2^{2+}$ complexes. *J. Am. Chem. Soc.* **2011**, *133* (32), 12767–12779.
- (23) Klug, C. M.; Cardenas, A. J. P.; Bullock, R. M.; O'Hagan, M.; Wiedner, E. S. Reversing the Tradeoff between Rate and Overpotential in Molecular Electrocatalysts for H_2 Production. *ACS Catal.* **2018**, *8* (4), 3286–3296.
- (24) Schreier, M.; Luo, J.; Gao, P.; Moehl, T.; Mayer, M. T.; Gratzel, M. Covalent Immobilization of a Molecular Catalyst on Cu₂O Photocathodes for CO₂ Reduction. *J. Am. Chem. Soc.* **2016**, *138* (6), 1938–46.
- (25) Brennan, B. J.; Llansola Portolés, M. J.; Liddell, P. A.; Moore, T. A.; Moore, A. L.; Gust, D. Comparison of silatrane, phosphonic acid, and carboxylic acid functional groups for attachment of porphyrin sensitizers to TiO₂ in photoelectrochemical cells. *Phys. Chem. Chem. Phys.* **2013**, *15* (39), 16605–16614.
- (26) Roevens, A.; Van Dijk, J. G.; Geldof, D.; Blockhuys, F.; Prelot, B.; Zajac, J.; Meynen, V. Aqueous or solvent based surface modification: The influence of the combination solvent – organic functional group on the surface characteristics of titanium dioxide grafted with organophosphonic acids. *Appl. Surf. Sci.* **2017**, *416*, 716–724.
- (27) Reynal, A.; Pastor, E.; Gross, M. A.; Selim, S.; Reisner, E.; Durrant, J. R. Unravelling the pH-dependence of a molecular photocatalytic system for hydrogen production. *Chem. Sci.* **2015**, *6* (8), 4855–4859.
- (28) Boschloo, G.; Fitzmaurice, D. Electron Accumulation in Nanostructured TiO₂ (Anatase) Electrodes. *J. Electrochem. Soc.* **2000**, *147* (3), 1117–1123.
- (29) Ryu, J.; Wuttig, A.; Surendranath, Y. Quantification of Interfacial pH Variation at Molecular Length Scales Using a Concurrent Non-Faradaic Reaction. *Angew. Chem., Int. Ed.* **2018**, *57* (30), 9300–9304.
- (30) Materna, K. L.; Crabtree, R. H.; Brudvig, G. W. Anchoring groups for photocatalytic water oxidation on metal oxide surfaces. *Chem. Soc. Rev.* **2017**, *46* (20), 6099–6110.
- (31) Cardenas, A. J. P.; Ginovska, B.; Kumar, N.; Hou, J.; Raugei, S.; Helm, M. L.; Appel, A. M.; Bullock, R. M.; O'Hagan, M. Controlling Proton Delivery through Catalyst Structural Dynamics. *Angew. Chem., Int. Ed.* **2016**, *55* (43), 13509–13513.
- (32) Hou, J.; Fang, M.; Cardenas, A. J. P.; Shaw, W. J.; Helm, M. L.; Bullock, R. M.; Roberts, J. A. S.; O'Hagan, M. Electrocatalytic H_2 production with a turnover frequency > 10⁷ s⁻¹: the medium provides an increase in rate but not overpotential. *Energy Environ. Sci.* **2014**, *7* (12), 4013–4017.
- (33) Bullock, R. M.; Das, A. K.; Appel, A. M. Surface Immobilization of Molecular Electrocatalysts for Energy Conversion. *Chem. - Eur. J.* **2017**, *23* (32), 7626–7641.
- (34) Coucouvanis, D. *Inorganic Syntheses, Volume 33*; Wiley, 2004.
- (35) Sheldrick, G. A short history of SHELX. *Acta Crystallogr., Sect. A: Found. Crystallogr.* **2008**, *64* (1), 112–122.
- (36) Dolomanov, O. V.; Bourhis, L. J.; Gildea, R. J.; Howard, J. A. K.; Puschmann, H. OLEX2: a complete structure solution, refinement and analysis program. *J. Appl. Crystallogr.* **2009**, *42* (2), 339–341.